ACT DR6 Insights on the Inflationary Attractor models and Reheating

Md Riajul Haque, 1, * Sourav Pal, 1, † and Debarun Paul 1, ‡

We investigate the observational constraints on α -attractor inflationary models and their post-inflationary reheating dynamics in light of the latest CMB data from ACT DR6 combined with Planck18, BICEP/Keck 2018, and DESI (collectively denoted P-ACT-LB-BK18). Focusing on both E- and T-type attractor potentials, we analyze how inflationary observables—namely the scalar spectral index n_s and the tensor-to-scalar ratio r—are indirectly influenced by reheating parameters such as the reheating temperature $T_{\rm RH}$, the inflaton equation-of-state w_ϕ , and the inflaton's couplings to Starndard Model particles. We incorporate indirect constraints from the overproduction of primordial gravitational waves (PGWs), particularly via $\Delta N_{\rm eff}$ bounds on BBN, which become significant for stiff post-inflationary dynamics. Our results show that E-models permit a wide range of reheating scenarios, including matter-like reheating ($w_\phi = 0$), while T-models are viable only for $w_\phi \gtrsim 0.44$. We derive bounds on inflaton—Standard Model couplings for both decay and scattering channels and identify parameter regimes compatible with recent ACT data for successful reheating. These findings establish a robust connection between inflationary theory, thermal history, and particle phenomenology, and provide predictive targets for future CMB missions.

12

CONTENTS

1.	Introduction	1
II.	Overview of the inflationary model	2
III.	Overview of Reheating Dynamics and Possible Scenarios	3
IV.	$\Delta N_{\rm eff}$ Constraints from PGWs	6
V.	Results A. Model Constraints $E{\text{-}model}$ $T{\text{-}model}$ B. Constraints on Coupling Parameters	8 8 8 8
VI.	Conclusions	11
	Acknowledgements	12

I. INTRODUCTION

The last decade has witnessed an unprecedented leap in our understanding of the early Universe, primarily driven by high-precision measurements of the cosmic microwave background (CMB) [1, 2]. Observations from Planck18, BICEP/Keck, and more recently, the Atacama Cosmology Telescope (ACT), have dramatically tightened constraints on the inflationary models. These advances not only refine our estimates of key inflationary observables,

References

such as the scalar spectral index n_s and the tensor-to-scalar ratio r, but also enable us to probe the microphysics underlying inflation [3–5] and its aftermath, particularly the reheating epoch [6–10].

Among the diverse landscape of inflationary frameworks, α -attractor models [11–18] have received considerable attention due to their strong theoretical underpinnings and robust predictive power. These models arise naturally in the contexts of supergravity and string theory, where the parameter α encapsulates the curvature of the scalar field manifold. By smoothly interpolating between chaotic inflation [19, 20] and plateau-like scenarios—such as Starobinsky inflation [21, 22]— α -attractors offer a unifying structure that encompasses a wide range of potentials. This makes them a compelling framework for connecting fundamental theory with cosmological observations.

The recent Data Release 6 (DR6) from the Atacama Cosmology Telescope (ACT) has provided improved measurements of the high- ℓ CMB power spectrum. When combined with Planck data (P-ACT), the scalar spectral index is constrained to $n_s = 0.9709 \pm 0.0038$ [23, 24]. Further inclusion of CMB lensing and Baryon Acoustic Oscillation (BAO) data from DESI (P-ACT-LB) refines the constraint to $n_s = 0.9743 \pm 0.0034$ [23, 24], which deviates from the Planck-only result at the 2σ level. This mild tension disfavors classic plateau models such as Starobinsky inflation, while favoring scenarios that predict slightly higher values of n_s , including α -attractor models. These updated constraints necessitate a renewed evaluation of the inflationary landscape, particularly for models that previously lay near the boundary of observational viability. Motivated by these developments, a variety of inflationary scenarios—such as warm inflation, Higgs inflation, and other theoretically motivated frameworks—have been revisited in the context of the recent ACT data [25–37].

However, the inflationary observables n_s and r alone are insufficient to fully reconstruct the dynamics of the early Universe. The reheating phase—during which the

¹ Physics and Applied Mathematics Unit, Indian Statistical Institute, 203 B.T. Road, Kolkata 700108, India

^{*} E-mail:riai.0009@gmail.com

[†] E-mail: soupal1729@gmail.com

[‡] E-mail: debarun31paul@gmail.com

inflaton decays and the Universe transitions into a hot, radiation-dominated era—plays a crucial intermediary role. It sets the initial conditions for Big Bang Nucleosynthesis (BBN), influences the number of inflationary e-folds between horizon exit of a given CMB pivot scale and the end of inflation, and affects the predicted values of n_s and r. Moreover, theoretical models of reheating establish a vital connection between inflation and particle physics via inflaton couplings to Standard Model (SM) or beyond-the-Standard-Model (BSM) fields. This phase is typically characterized by two key parameters: the reheating temperature (T_{RH}) and the effective equation of state (w_{ϕ}) . The reheating temperature depends sensitively on both the inflaton's coupling to SM and the structure of the inflaton potential $V(\phi)$ near its minimum—often determined by the exponent in the potential.

In this work, we consider reheating scenarios in which the inflaton decays into either fermions $(\phi \to \bar{f}f)$ or bosons $(\phi \to bb)$, as well as scattering processes such as $\phi\phi \to bb$ [38–40]. The decay products are assumed to be massless and rapidly thermalize, contributing to the radiation bath. Due to the absence of direct observational probes of this epoch, the reheating temperature $T_{\rm BH}$ remains poorly constrained. It is bounded from above by the energy scale allowed by CMB observations, corresponding to instantaneous reheating ($\sim 10^{15}$ GeV), and from below by the minimum temperature required for successful BBN $(T_{\rm BBN} \sim 4 {\rm MeV})$ [41–43]. While the standard inflationary observables (n_s, r) are shaped by both inflationary and post-inflationary dynamics, the details of reheating encode complementary information—particularly about fundamental couplings between the inflaton and SM particles [38–40, 44–51].

Recently, there have been growing efforts to constrain reheating parameters using BICEP/Keck 2018 (BK18) data in combination with Planck18 observations [52-54]. In this paper, we explore constraints on both the α -attractor model parameters, reheating parameters—including $T_{\rm RH}$, the inflaton equation of state w_{ϕ} , and inflaton couplings—using the latest ACT DR6 data in combination with Planck18, BK18, and DESI. Additionally, we incorporate an independent constraint arising from the overproduction of primordial gravitational waves (PGWs). The PGWs correspond to tensor perturbations generated due to vacuum fluctuations during inflation [55–60]. The dynamics of reheating leave imprints on the stochastic background of these PGWs, particularly in modes that re-enter the horizon during this phase [61–66]. A stiff equation of state $(w_{\phi} \geq 1/3)$ leads to a blue-tilted GW spectrum, potentially resulting in an excess of high-frequency GWs. These excess PGWs contribute to the effective number of relativistic degrees of freedom, $\Delta N_{\rm eff}$, which is constrained by both BBN and CMB data. Consequently, $\Delta N_{\rm eff}$ bounds ¹ offer an indirect probe of reheating physics, allowing us to place

a lower bound on the reheating temperature $T_{\rm RH}$ for stiff post-inflationary dynamics.

This work is motivated by the synergy between recent ACT DR6 measurements and theoretical developments in inflationary reheating. Our main objectives are as follows:

- To analyze the viability of α -attractor models—both E- and T-type—in light of updated constraints on n_s and r from the combination of Planck18, ACT, DESI, and BICEP/Keck data.
- To explore the implications of various reheating scenarios, parametrized by different equations of state and inflaton decay channels, on the inflationary parameter space.
- To incorporate indirect constraints on the reheating temperature arising from the overproduction of primordial gravitational waves (PGWs), particularly through bounds on the effective number of relativistic species, $\Delta N_{\rm eff}$.
- To derive bounds on inflaton couplings to bosonic and fermionic particles, which determine the efficiency of reheating and shape the subsequent thermal history of the Universe.

The structure of the paper is as follows. In Sec. II, we provide an overview of the inflationary framework, focusing on the α -attractor models. Section III presents a detailed analysis of the reheating phase, including inflaton decay via fermionic and bosonic channels. In Sec. IV, we investigate constraints on the reheating temperature and inflaton equation of state arising from the overproduction of PGWs. Section V presents our main results, including constraints on the inflaton potential parameters and associated reheating quantities, $T_{\rm RH}$ and w_{ϕ} , based on ACT DR6 data. Finally, Sec. VI summarizes our findings and outlines directions for future research.

II. OVERVIEW OF THE INFLATIONARY MODEL

In the context of canonical single-field inflationary theories, two well-studied frameworks, the T-model and the E-model describe the dynamics of the inflaton through attractor-type potentials. These models are characterized by the scalar potentials,

$$V(\phi) = \begin{cases} \Lambda^4 \left[1 - e^{-\sqrt{\frac{2}{3\alpha}}\phi/M_{\rm P}} \right]^{2n}, & \text{E-model}, \\ \Lambda^4 \left[\tanh\left(\frac{\phi}{\sqrt{6\alpha}M_{\rm P}}\right) \right]^{2n}, & \text{T-model}. \end{cases}$$
(1)

straints on the effective number of relativistic species, $\Delta N_{\rm eff}$, we refer the reader to Table II of Ref. [67]. In this analysis, however, we adopt the P-ACT-LB bound, which imposes a constraint of $\Delta N_{\rm eff} < 0.17$ [23, 24] at 95% C.L.

¹ For a comprehensive summary of current and predicted con-

Here, Λ denotes the inflationary energy scale, n is index of the potential controlling the steepness near its minimum, and α is a dimensionless parameter shaping the curvature of the potential ². These model parameters can be essentially determined from the scalar curvature perturbations generated during inflation, characterized by the power spectrum $\Delta_{\mathcal{R}}^2 = A_{\mathcal{R}} (k/k_*)^{n_s-1}$. Here, $A_{\mathcal{R}}$ is the amplitude of scalar fluctuations and n_s is the scalar spectral index. k_* is the pivot scale which is considered to be $0.05\,\mathrm{Mpc}^{-1}$ throughout our analysis. Another key CMB observable is the tensor-to-scalar ratio, defined as $r \equiv A_{\mathcal{T}}/A_{\mathcal{R}}$, where $A_{\mathcal{T}}$ denotes the amplitude of the tensor power spectrum. The tensor spectrum is typically nearly scale-invariant, arising from quantum fluctuations of the gravitational field during inflation. For any canonical single field inflationary model, the slow-roll parameters can be defined as,

$$\epsilon \equiv \frac{1}{2} M_{\rm p}^2 \left(\frac{V'}{V}\right)^2 \,, \qquad \eta \equiv M_{\rm p}^2 \left(\frac{V''}{V}\right) \,, \eqno(2)$$

where prime denotes derivative with respect to ϕ . Furthermore, under the slow-roll approximation, CMB observables $(n_s, r \text{ and } A_s)$ can be expressed in terms of the slow-roll parameters as follows,

$$n_s = 1 - 6\epsilon(\phi) + 2\eta(\phi)$$
, $r = 16\epsilon(\phi)$. (3)

Subsequent dynamics of the inflaton field is governed by the inflationary energy scale /Hubble parameter (H_k) , which can be approximated in terms or r and $A_{\mathcal{R}}$ as follows,

$$H_{\rm k} = \frac{\pi M_{\rm P} \sqrt{r A_{\mathcal{R}}}}{\sqrt{2}} \simeq \sqrt{\frac{V(\phi_{\rm k})}{3M_{\rm P}^2}}.$$
 (4)

The duration of inflation can be parametrized by the total e-folds number (N_k) between the horizon crossing of the CMB mode with comoving number k and the end of inflation. For the α -attractor model, N_k is given by [38, 68, 69],

$$N_{k} = \begin{cases} \frac{3\alpha}{4n} \left(\exp \sqrt{\frac{2}{3\alpha}} \frac{\phi_{k}}{M_{P}} - \exp \sqrt{\frac{2}{3\alpha}} \frac{\phi_{\text{end}}}{M_{P}} \right) \\ -\sqrt{\frac{3\alpha}{8n^{2}M_{P}^{2}}} (\phi_{k} - \phi_{\text{end}}), & \text{E - model}, \\ \frac{3\alpha}{4n} \left(\cosh \sqrt{\frac{2}{3\alpha}} \frac{\phi_{k}}{M_{P}} - \cosh \sqrt{\frac{2}{3\alpha}} \frac{\phi_{\text{end}}}{M_{P}} \right) & \text{T - model}, \end{cases}$$

$$(5)$$

where ϕ_k and $\phi_{\rm end}$ are field values at the time of horizon crossing and at the end of inflation respectively. One can obtain the value of Λ in the large field limit by setting $\Lambda^4 \approx V(\phi_k)$. More general expressions for ϕ_k and Λ can be found in [68] for the E-model, and in [38] for the T-model. The end of the inflation is marked by the condition

 $\epsilon(\phi_{\rm end}) = 1$. Finally the tensor-to-scalar ratio, r can be expressed in terms of the α -attractor model parameters as follows [38, 68, 69],

$$r = \begin{cases} \frac{64n^2}{3\alpha} \left(e^{\sqrt{\frac{2}{3\alpha}} \frac{\phi_k}{M_P}} - 1 \right)^{-2}, & \text{E-model,} \\ \frac{64n^2}{3\alpha} \operatorname{csch}^2 \left(\sqrt{\frac{2}{3\alpha}} \frac{\phi_k}{M_P} \right), & \text{T-model.} \end{cases}$$
(6)

After inflation, the Universe is cold, dark, and dominated by the homogeneous inflaton field. A natural consequence of this state is the decay of the inflaton into Standard Model particles, thereby reheating the Universe and initiating a radiation-dominated era—an essential condition for the onset of Big Bang Nucleosynthesis (BBN). The inflaton energy density at the end of inflation can be approximated as [38, 54],

$$\rho_{\phi}^{\text{end}} \sim \frac{\Lambda^4}{\alpha_1^{2n}} \left[\frac{\phi_{\text{end}}}{M_{\text{P}}} \right]^{2n},$$
(7)

where $\alpha_1 \equiv (\sqrt{3\alpha/2}, \sqrt{6\alpha})$ for E-model and T-model, respectively. This relation allows us to connect the inflationary era with the subsequent evolution during the post-inflationary epoch, namely the reheating phase. Let us now briefly discuss the reheating phase, highlighting how various non-gravitational couplings influence both the duration of reheating and the temperature at its conclusion—commonly referred to as the reheating temperature $T_{\rm RH}$.

III. OVERVIEW OF REHEATING DYNAMICS AND POSSIBLE SCENARIOS

Following the end of inflation, the inflaton field undergoes coherent oscillations around the minimum of its potential. The potential near this minimum behaves as $V(\phi) \sim \phi^{2n}$ for the α -attractor models considered here. These oscillations mark the beginning of the reheating era, where the inflaton decays into SM particles, gradually transitioning the Universe into a radiation-dominated (RD) phase.

The inflaton field that oscillates coherently, may be broken down into

$$\phi(t) = \phi_0(t)\mathcal{P}(t),\tag{8}$$

where $\phi_0(t)$ denotes the slowly varying envelope, incorporating the effects of redshifts, and $\mathcal{P}(t)$, a quasi-periodic function, describes the short timescale oscillation of the potential with Fourier expansion $\mathcal{P}(t) = \sum_{\mu=-\infty}^{\infty} \mathcal{P}_{\mu} e^{i\mu\omega t}$. The oscillation frequency is given by [38]

$$\omega = m_{\phi}(t) \sqrt{\frac{\pi n}{(2n-1)}} \frac{\Gamma\left(\frac{1}{2} + \frac{1}{2n}\right)}{\Gamma\left(\frac{1}{2n}\right)},\tag{9}$$

where m_{ϕ} is the mass of the inflaton, which can defined as,

$$m_{\phi}(t) \equiv \sqrt{V''(\phi_0(t))} \propto \phi_0(t)^{2(n-1)}.$$
 (10)

 $^{^2}$ Note that $M_{\rm P}$ is the reduced Planck mass, defined as $M_{\rm P}=\frac{1}{\sqrt{8\pi G}}=2.43\times 10^{18}\,{\rm GeV}.$

Assuming that the oscillation period is much shorter than the timescales associated with redshift and decay, averaging over a single oscillation yields an inflaton energy density approximately given by $\rho_{\phi} \sim V(\phi_0)$, and determines the effective average equation of state (EoS) [38, 70]

$$w_{\phi} \simeq \frac{n-1}{n+1}.\tag{11}$$

Considering that the inflaton decays only into the radiation, the Boltzmann equation for the energy density of inflaton (ρ_{ϕ}) and radiation (ρ_{R}) can be expressed as

$$\dot{\rho}_{\phi} + 3H(1+w_{\phi})\rho_{\phi} = -\Gamma_{\phi}(t)(1+w_{\phi})\rho_{\phi},$$
 (12)

$$\dot{\rho}_R + 4H\rho_R = \Gamma_\phi(t)(1+w_\phi)\rho_\phi,\tag{13}$$

with $\Gamma_{\phi}(t)$ being the time dependent decay rate of inflaton. The corresponding Hubble rate can be determined as follows:

$$H^2 = \frac{\rho_\phi + \rho_R}{3M_{\rm P}^2}. (14)$$

Reheating phase ends when $\rho_{\phi} \simeq \rho_R$, where the equality marks the temperature of reheating $(T_{\rm RH})$ with corresponding scale factor $a_{\rm RH}$. For analytical estimation, Boltzmann equations (Eqs. (12) and (13)) provides $\rho \sim a^{-3(1+w_{\phi})}$ and $\rho_R \sim a^{-4}$. Thus, the radiation temperature at the end of reheating—i.e., the reheating temperature—can be expressed as

$$T_{\rm RH} \simeq \left(\frac{90M_{\rm p}^2 H_{\rm end}^2}{\pi^2 g_{*RH}}\right)^{1/4} e^{-\frac{3}{4}N_{\rm RH}(1+w_{\phi})},$$
 (15)

Here, $N_{\rm RH}$ denotes the number of e-folds between the end of inflation and the end of the reheating phase. The case $N_{\rm RH}=0$ corresponds to an instantaneous reheating scenario. The quantity $g_{*{\rm RH}}$ represents the effective number of relativistic degrees of freedom in the thermal bath at the end of reheating. Under the standard assumption, the comoving entropy density of the Universe is conserved from the end of reheating until the present-day. Thus, assuming the conservation of comoving entropy density, the reheating temperature can be connected with the present-day temperature of the Universe T_0 (= 2.725 K) as [71, 72]

$$T_{\rm RH} = \left(\frac{43}{11g_{*S,\rm RH}}\right)^{1/3} T_0 \frac{H_{\rm k}}{k_*} e^{-(N_k + N_{\rm RH})},$$
 (16)

where N_k denotes the number of e-folds between the end of inflation and the horizon exit of a given CMB pivot scale, k_* . $g_{*S,RH}$ is the relativistic degree for freedom associated with the entropy calculated at the end of reheating. Upon comparison of Eq. (15) and Eq. (16), N_k can be written in terms of reheating temperature as

$$N_{k} = \log \left[\left(\frac{43}{11g_{*S,RH}} \right)^{1/3} T_{0} \frac{H_{k}}{k_{*}} \right] \times T_{RH}^{\frac{4}{3(1+w_{\phi})}-1} \left(\frac{\pi^{2}g_{*RH}}{90M_{P}^{2}H_{end}^{2}} \right)^{\frac{1}{3(1+w_{\phi})}} \right]$$
(17)

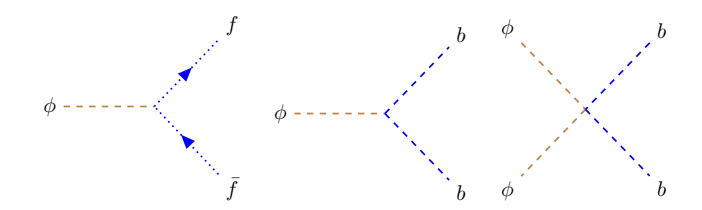


FIG. 1: Feynman diagrams for the decay of inflaton into fermions and bosons, and annihilation into bosons.

Depending on how the inflaton couples to other fields, reheating can proceed via non-gravitational interactions. These interactions are governed by specific decay or annihilation processes involving the inflaton, which is illustrated by the Feynman diagram in Fig. 1. The corresponding interaction Lagrangian for such non-gravitational interactions can be written as [38]

$$\mathcal{L}_{\text{int}} \supset \begin{cases} y_{\phi}\phi\bar{f}f & \phi \to \bar{f}f \\ g_{\phi}\phi bb & \phi \to bb \\ \sigma_{\phi}\phi^{2}b^{2} & \phi\phi \to bb \end{cases}$$
(18)

with f and b being the fermionic and basonic fields, respectively, however, this can be extended for more inflaton-matter/radiation coupling in a very straightforward fashion. The coupling y_{ϕ} and σ_{ϕ} are the dimensionless Yukawa-like coupling and four-point coupling, respectively, whereas, g_{ϕ} is the dimensionful bosonic coupling. The corresponding decay/annihilation rate of the aforementioned interactions can be expressed as [38]

$$\Gamma_{\phi}(t) \equiv \begin{cases}
\frac{y_{\text{eff}}^2 m_{\phi}(t)}{8\pi}, & \phi \to \bar{f}f, \\
\frac{g_{\text{eff}}^2}{8\pi m_{\phi}(t)}, & \phi \to bb, \\
\frac{\sigma_{\text{eff}}^2}{8\pi \frac{p_{\phi}(t)}{m_{\phi}^3(t)}}, & \phi\phi \to bb.
\end{cases}$$
(19)

The 'eff' at the suffix represents the effective coupling over oscillation average. The effective coupling defers from standard coupling because for n > 1, the inflaton mass becomes time-dependent due to the oscillatory behavior of the field $\phi(t)$ (see Eq. (10)). The ratio of the oscillation-induced effective coupling parameters to their corresponding Lagrangian values can be estimated as [38]

$$\left(\frac{y_{\text{eff}}}{y_{\phi}}\right)^{2} = 2(n+1)(2n-1) \left(\frac{w}{m_{\phi}}\right)^{3} \sum_{\mu=1}^{\infty} \mu^{3} |\mathcal{P}_{\mu}|^{2}, (20)$$

$$\left(\frac{g_{\text{eff}}}{g_{\phi}}\right)^{2} = 2(n+1)(2n-1)\frac{w}{m_{\phi}}\sum_{\mu=1}^{\infty}\mu\,|\mathcal{P}_{\mu}|^{2}\,,\tag{21}$$

$$\left(\frac{\sigma_{\text{eff}}}{\sigma_{\phi}}\right)^{2} = 4n (n+1) (2n-1)^{2} \frac{w}{m_{\phi}} \sum_{\mu=1}^{\infty} \mu |(\mathcal{P}^{2})_{\mu}|^{2}. (22)$$

The authors of [64] provides the numerical values for the effective coupling for different EoS with corresponding Fourier sum, which is displayed in Table I.

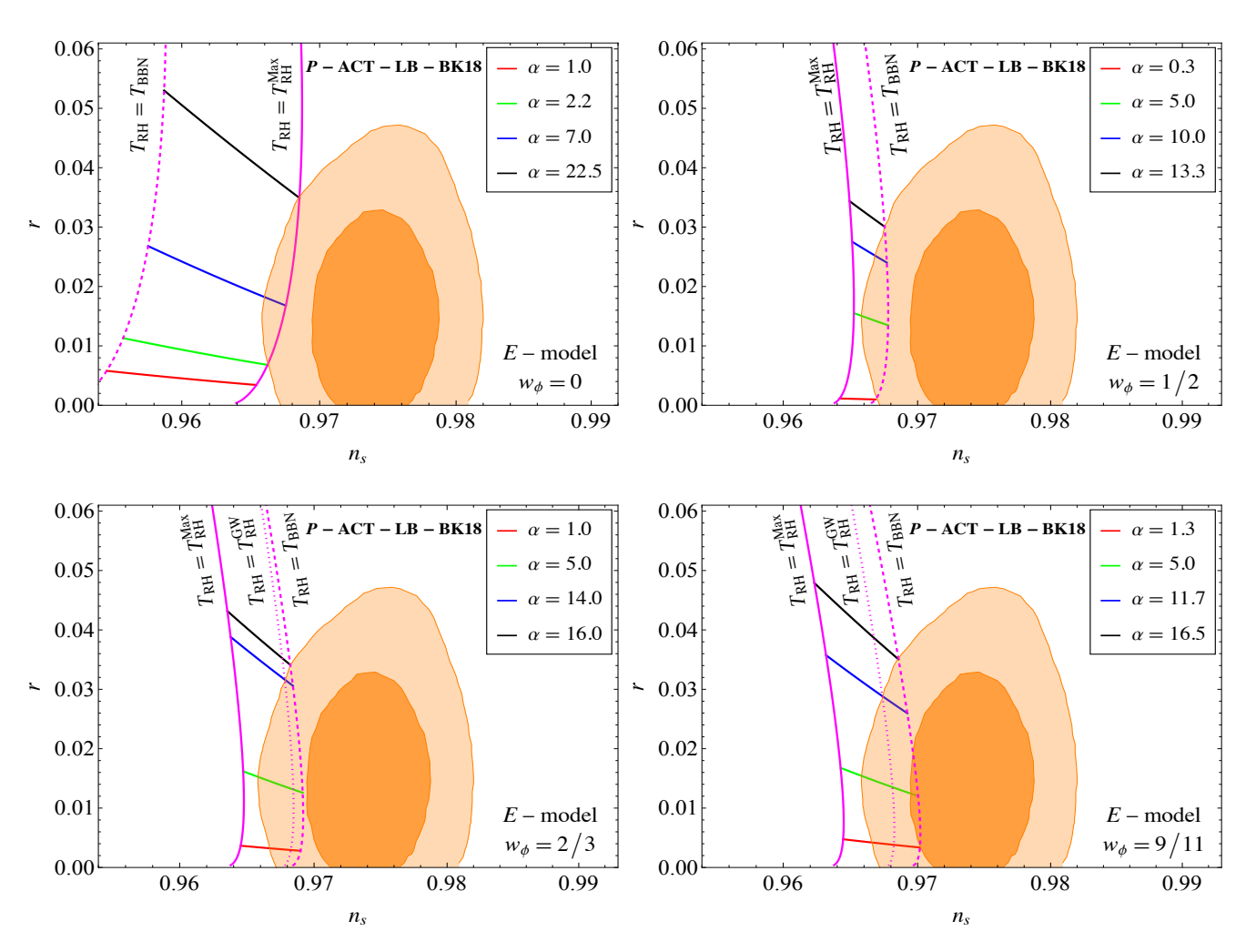


FIG. 2: Predictions of the α -attractor E-model for various combinations of (α, w_{ϕ}) are shown projected onto the (n_s, r) plane, overlaid with the latest combined constraints from P-ACT-LB-BK18. Both n_s and r are projected for $k_* = 0.05 \, \mathrm{Mpc}^{-1}$. The deep and light orange shaded regions indicate the 1σ (68% C.L.) and 2σ (95% C.L.) confidence intervals, respectively. The reheating temperature spans from T_{BBN} to $T_{\mathrm{RH}}^{\mathrm{Max}}$, represented by dashed and solid magenta lines. An additional critical temperature scale, $T_{\mathrm{RH}}^{\mathrm{GW}}$, is marked by a dotted magenta line, which is derived from ΔN_{eff} constraints on the overproduction of PGWs.

$n\left(w_{\phi} ight)$	$\sum \mu^3 \mathcal{P}_{\mu} ^2$	$\sum \mu \mathcal{P}_{\mu} ^2$	$\sum \mu (\mathcal{P}^2)_{\mu} ^2$	$\frac{y_{\mathrm{eff}}}{y_{\phi}}$	$\frac{g_{\mathrm{eff}}}{g_{\phi}}$	$\frac{\sigma_{\mathrm{eff}}}{\sigma_{\phi}}$
1(0)	$\frac{1}{4}$	$\frac{1}{4}$	$\frac{1}{8}$	1	1	1
$2\left(\frac{1}{3}\right)$	0.241	0.229	0.125	0.71	1.42	3.64
$5\left(\frac{2}{3}\right)$	0.257	0.205	0.120	0.50	2.14	15.6
$7\left(\frac{3}{4}\right)$	0.270	0.198	0.117	0.44	2.49	25.8
$10\left(\frac{9}{11}\right)$	0.287	0.191	0.114	0.38	2.92	44.0

TABLE I: Numerical values for the effective couplings and the Fourier sums.

Using the expression of m_{ϕ} (Eq. (10)), one can rewritten

Eq. (19) as follows [38]:

$$\Gamma_{\phi}(t) \equiv \gamma_{\phi}(t) \left(\frac{\rho_{\phi}}{M_{\rm p}^4}\right)^l,$$
 (23)

with

$$\gamma_{\phi}(t), \ l \equiv \begin{cases} \frac{y_{\rm eff}^2 \sqrt{2n \, (2n-1)} \, \lambda^{1/2n} \, M_{\rm P}}{8\pi}, & \frac{1}{2} - \frac{1}{2n} & \text{for } \phi \to \bar{f}f \,, \\ \frac{g_{\rm eff}^2}{8\pi \, \sqrt{2n \, (2n-1)} \, \lambda^{1/2n} \, M_{\rm P}}, & \frac{1}{2n} - \frac{1}{2} & \text{for } \phi \to bb \,, \, (24) \\ \frac{\sigma_{\rm eff}^2 \, M_{\rm P}}{8\pi \, (2n \, (2n-1))^{3/2} \, \lambda^{3/2n}}, & \frac{3}{2n} - \frac{1}{2} & \text{for } \phi \phi \to bb \,. \end{cases}$$

Thus, in terms of the interaction rates, the reheating temperature can be estimated as [38]

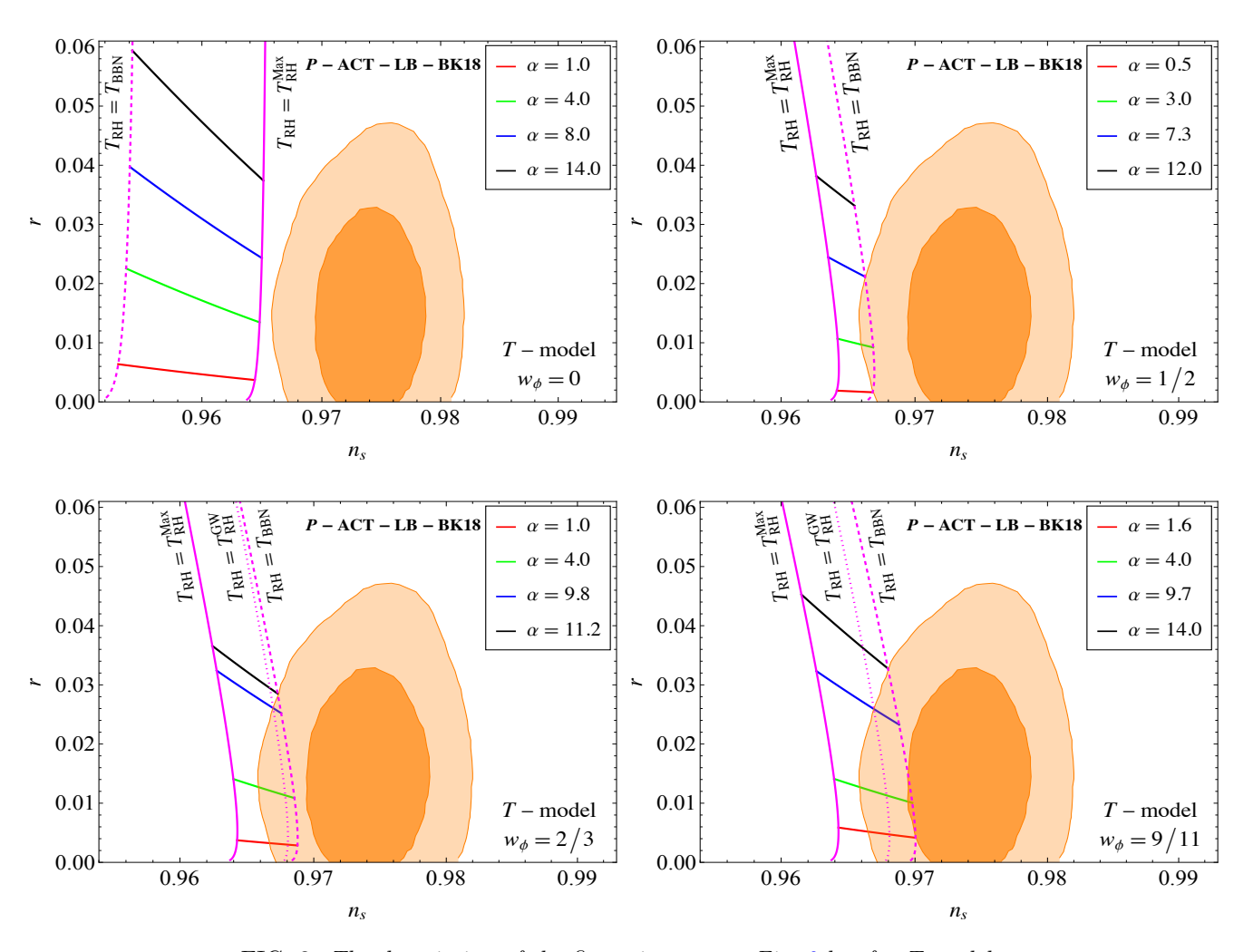


FIG. 3: The description of the figure is same as Fig. 2 but for T-model.

$$T_{\rm RH} = \begin{cases} \left(\frac{30}{\pi^2 g_{*,\rm RH}}\right)^{1/4} \left(\frac{n+4-6nl}{2n} \frac{M_{\rm P}^{4l-1}}{\sqrt{3}\gamma_{\phi}}\right)^{\frac{1}{2(2l-1)}} & \text{for } 4+n-6nl > 0, \\ \left(\frac{30}{\pi^2 g_{*,\rm RH}}\right)^{1/4} \rho_{\rm end}^{\frac{6nl-n-4}{8(n-2)}} \left(\frac{6nl-n-4}{2n} \frac{M_{\rm P}^{4l-1}}{\sqrt{3}\gamma_{\phi}}\right)^{-\frac{3n}{4(n-2)}} & \text{for } 4+n-6nl < 0. \end{cases}$$
 (25)

Thus, by comparing Eqs. (17) and (25), one can establish a connection between the coupling parameters and the inflationary parameters, which will be comprehensively analyzed in Sec. V. The reheating temperature, in principle, can be directly probed through the observations of the primordial gravitational wave (PGW) background. However, the constraints on PGWs arises from the bounds on the effective number of relativistic species ($\Delta N_{\rm eff}$) of the Universe, impose limits the measurement of the reheating temperature. These constraints will be explored in detail in the following section.

IV. $\Delta N_{\rm eff}$ CONSTRAINTS FROM PGWS

In this section, we explore the constraints arising from spectral energy density of PGWs generated by first-order tensor perturbations during the inflationary era, within the minimal setup-that is, in absence of any source terms. As already mentioned, the primary observational constraint on PGWs comes from measurements of the tensor-to-scalar ratio r at the pivot scale k_* , derived from CMB data . In α -attractor models, the PGW spectrum is found to be nearly scale-invariant, as shown in detail in [60]. The amplitude and shape of the PGW spectral energy density are primarily determined by the energy scale of inflation.

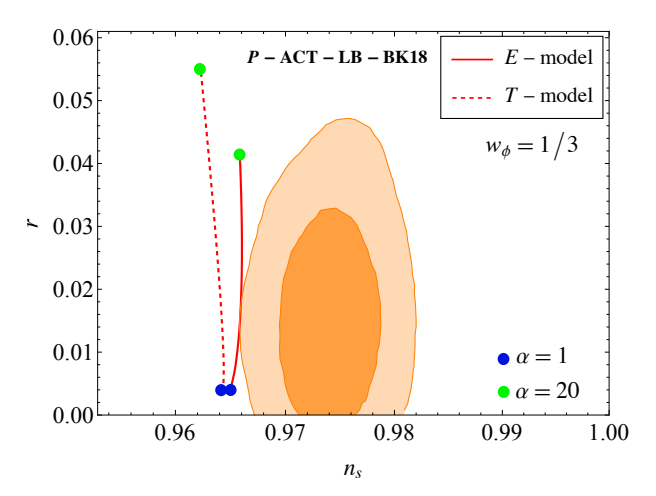


FIG. 4: Predictions of both α -attractor E- and T-model for $w_{\phi} = 1/3$ are shown projected onto the (n_s, r) plane, overlaid with the latest combined constraints from P-ACT-LB-BK18. The deep and light orange shaded regions indicate the 1σ (68% C.L.) and 2σ (95% C.L.) confidence intervals, respectively. Both n_s and r are projected for $k_* = 0.05 \,\mathrm{Mpc}^{-1}$.

To predict the present-day spectral energy density of modes that re-enter the horizon during the reheating era, one must consistently track the evolution of individual perturbation modes through the reheating phase following inflation. The inflation scale is directly related to r and the amplitude $A_{\mathcal{R}}$ of the scalar perturbation. Focusing on modes $(k < k_{\rm RH})$ that re-enter the horizon during radiation domination, the present-day dimensionless spectral energy density of PGWs is given by,

$$\Omega_{\rm GW}^{(0)}(k) h^2 = \Omega_{\rm R}^{(0)} h^2 \frac{H_{\rm end}^2}{12 \pi^2 M_{\rm P}^2}
= 3.5 \times 10^{-17} \left(\frac{H_{\rm end}}{10^{-5} M_{\rm P}} \right)^2, \quad (26)$$

where we have used the present-day radiation density $\Omega_{\rm R}^{(0)} h^2 = 4.16 \times 10^{-5}$ including contributions from both photons and three neutrino species. If reheating phase precedes radiation domination, then modes in the intermediate range, $k_{\rm RH} < k < k_{\rm end}$ re-enter the horizon during reheating. In general, $k_{\rm RH}$ is determined by the equation of state (EoS) during reheating (w_{ϕ}) and the reheating temperature (T_{RH}) , whereas the wavenumber k_{end} is primarily governed by $H_{\rm end}$. Thus the GW spectral energy density accounting the effects of perturbation modes that re-enter the Hubble radius during the epoch of reheating is given by (see Ref. [62] for detailed calculations),

$$\Omega_{\rm GW}^{(0)}(k) h^2 \simeq \Omega_R^{(0)} h^2 \frac{H_{\rm end}^2}{12 \pi^2 M_{\rm P}^2} \frac{\mu(w_\phi)}{\pi} \left(\frac{k}{k_{\rm RH}}\right)^{n_{w_\phi}}$$

$$\simeq 3.5 \times 10^{-17} \left(\frac{H_{\rm end}}{10^{-5} M_{\rm P}}\right)^2 \frac{\mu(w_\phi)}{\pi} \left(\frac{k}{k_{\rm RH}}\right)^{n_{w_\phi}}$$
(27)

where the quantity $\mu(w_{\phi})$ and the index $n_{w_{\phi}}$ are given

$$\mu(w_{\phi}) \equiv (1 + 3 w_{\phi})^{4/(1+3 w_{\phi})} \Gamma^{2} \left(\frac{5 + 3 w_{\phi}}{2 + 6 w_{\phi}} \right),$$

$$n_{w_{\phi}} \equiv -\frac{2(1 - 3 w_{\phi})}{1 + 3 w_{\phi}}.$$
(28)

While $\mu(w_{\phi}) \simeq \mathcal{O}(1)$ for $0 \leq w_{\phi} \leq 1$, the tilt $n_{w_{\phi}}$ becomes positive or negative depending on whether $w_{\phi} > 1/3$ or $w_{\phi} < 1/3$, and vanishes at radiation domination $(w_{\phi} = 1/3)$. Moreover, the wave number $k_{\rm end}$ can be approximately expressed in terms of the inflationary energy scale $H_{\rm end}$ and the reheating parameters $T_{\rm RH}$ as,

$$k_{\text{end}} = a_{\text{end}} H_{\text{end}} \simeq H_{\text{end}} \frac{T_0}{T_{\text{RH}}} \left(\frac{43}{11 g_{*S,\text{RH}}}\right)^{1/3} \times \left(\frac{\pi^2 g_{*\text{RH}} T_{\text{RH}}^4}{90 M_{\text{P}}^2 H_{\text{end}}^2}\right)^{1/[3 (1+w_{\phi})]}.$$
 (29)

On the other hand, the effective number of additional relativistic degrees of freedom (which is generally quantified by $\Delta N_{\rm eff}$) at the epoch of BBN, places tighter constraints on the reheating temperature. High-frequency GWs behave like additional relativistic degrees of freedom and contribute to total $\Delta N_{\rm eff}$. However, $\Delta N_{\rm eff}$ is tightly constrained by the recent ACT data, $\Delta N_{\rm eff} \leq 0.17$ with 95% C.L.[23, 24]. Following [54, 63], the constraint equation on PGW in terms of $\Delta N_{\rm eff}$ is given by,

$$\int_{k_{\text{RH}}}^{k_{\text{end}}} \frac{\mathrm{d}k}{k} \,\Omega_{\text{GW}}^{(0)}(k) \, h^2 \le \frac{7}{8} \, \left(\frac{4}{11}\right)^{4/3} \, \Omega_{\gamma}^{(0)} \, h^2 \, \Delta N_{\text{eff}}, \tag{30}$$

where $\Omega_{\gamma}^{(0)} h^2 \simeq 2.47 \times 10^{-5}$ represents the present-day energy density of photons. The above constraint is of particular interest whenever $w_{\phi} > 1/3$, as spectral energy density of PGW has positive value for modes with k > $k_{\rm RH}$. Upon using the form of $\Omega_{\rm GW}^{(0)}$ in Eq. (27), the above condition reduces to,

$$\Omega_R^{(0)} h^2 \frac{H_{\text{end}}^2}{12 \pi^2 M_{\text{P}}^2} \frac{\mu(w_\phi) (1 + 3 w_\phi)}{2 \pi (3 w_\phi - 1)} \left(\frac{k_{\text{end}}}{k_{\text{RH}}}\right)^{\frac{6 w_\phi - 2}{1 + 3 w_\phi}} \\
\leq 5.61 \times 10^{-6} \Delta N_{\text{eff}}. (31)$$

The ratio between k_{end} and k_{RH} in the above equation can be further expressed as,

$$\frac{k_{\text{end}}}{k_{\text{RH}}} = \left(\frac{90 H_{\text{end}}^2 M_{\text{p}}^2}{\pi^2 g_{*\text{RH}}}\right)^{\frac{(1+3 w_{\phi})}{[6(1+w_{\phi})]}} T_{\text{RH}}^{-2(1+3 w_{\phi})/[3(1+w_{\phi})]}.$$
(32)

Combining Eqs. (30), (31) and (32), one can arrive at the following bound on the reheating temperature $T_{\rm RH}$,

$$\frac{F}{2} \simeq \Omega_{R}^{(0)} h^{2} \frac{H_{\text{end}}}{12 \pi^{2} M_{\text{P}}^{2}} \frac{\mu(w_{\phi})}{\pi} \left(\frac{k}{k_{\text{RH}}}\right)^{n_{\psi}} \left(\frac{k}{k_{\text{RH}}}\right)^{n_{\psi}} \qquad T_{\text{RH}} \geq \left[\frac{\Omega_{R}^{(0)} h^{2}}{5.61 \times 10^{-6} \Delta N_{\text{eff}}} \frac{H_{\text{end}}^{2}}{12 \pi^{2} M_{\text{P}}^{2}} \frac{\mu(w_{\phi}) (1+3 w_{\phi})}{2 \pi (3 w_{\phi}-1)}\right]^{\frac{3(1+w_{\phi})}{4(3 w_{\phi}-1)}} \simeq 3.5 \times 10^{-17} \left(\frac{H_{\text{end}}}{10^{-5} M_{\text{P}}}\right)^{2} \frac{\mu(w_{\phi})}{\pi} \left(\frac{k}{k_{\text{RH}}}\right)^{n_{\psi}}, \qquad \times \left(\frac{90 H_{\text{end}}^{2} M_{\text{P}}^{2}}{\pi^{2} g_{*\text{RH}}}\right)^{\frac{1}{4}} \equiv T_{\text{RH}}^{\text{GW}}. \tag{33}$$

Taking $T_{\rm RH}^{\rm GW} \sim T_{\rm BBN} \approx 4\,{\rm MeV}$, we observe that the BBN constraint on PGWs becomes relevant only if $w_{\phi} \geq 0.6$. This threshold defines a new lower bound on the reheating temperature due to PGWs, denoted as $T_{\rm RH}^{\rm GW}$. The above condition implies that for particular values of $(w_{\phi}, T_{\rm RH})$, the upper bound on $\Delta N_{\rm eff}$ constrains the energy scale of inflation or equivalently imposes a constraint on r. This further puts constraint on the coupling parameters.

V. RESULTS

This section presents the observational constraints on the α -attractor inflationary models and their associated reheating dynamics. We focus on how the inflationary observables (n_s, r) are related to the number of e-foldings N_k , which in turn depends on the reheating temperature $T_{\rm RH}$. These observables are expressed in terms of the inflationary model parameters α and n, establishing a direct link between the inflationary dynamics and post-inflationary reheating. In particular, since the number of e-foldings is sensitive to the thermal history following inflation, we use Eqs. (5) and (17) simultaneously to evaluate n_s in terms of α , n and $T_{\rm RH}$, thereby enabling constraints on these parameters using current data.

Furthermore, the reheating temperature is connected to the inflaton–SM coupling via Eq. (25) and, allowing for a joint constraint on both the inflationary potential and the coupling strength. Our analysis incorporates the most recent observational data, including Planck18 with lensing, ACT DR6, BAO from DESI, and BICEP/Keck 2018 (collectively denoted as P-ACT-LB-BK18)³. These datasets provide tight constraints on n_s and r, which in turn translate into bounds on the reheating temperature and the microphysics of reheating i.e., the coupling between the inflaton and SM particles.

A. Model Constraints

E-model

Figs. 2, 4 and 5 illustrate the predictions of the E-model in the (n_s, r) plane for various combinations of the parameter α and the reheating EoS parameter w_{ϕ} . For reheating scenarios with $w_{\phi} < 1/3$, the combined current dataset P-ACT-LB-BK18 imposes a lower bound on the reheating temperature, while the upper bound is determined by the assumption of instantaneous reheating. Conversely, for $w_{\phi} > 1/3$, the situation is reversed. The upper bound on the reheating temperature is set by the aforementioned dataset, whereas the lower bound is fixed by BBN or limits on the effective number of relativistic species $\Delta N_{\rm eff}$ considering the overproduction of the PGWs. For the

T-model

Figs. 3, 4 and 5 present the corresponding results for the T-model. A key distinction from the E-model is that, the case with $w_{\phi} \leq 1/3$ is entirely excluded at the 2σ level at any values of α . The T-model enters the 2σ confidence region only for $w_{\phi} \gtrsim 0.44$, with the best fit occurring around $\alpha \sim 4$. This indicates a strong preference for a relatively stiff post-inflationary EoS within this class of models. As shown in Fig. 5 (top right), the T-model allows slightly lower maximum reheating temperatures compared to the E-model. For example, at $w_{\phi} = 9/11$, the E-model permits reheating temperatures up to 5×10^{11} GeV, whereas the T-model allows slightly lower temperatures approximately 10¹¹ GeV. As in the E-model, the stiff EoS in the T-model trigger constraints from the overproduction of PGWs, which raise the lower bound on the reheating temperature beyond the BBN threshold. Consequently, the allowed parameter space for α , N_k , and $T_{\rm RH}$ is narrower in the T-model compared to the E-model. Numerical bounds on these parameters for different w_{ϕ} are tabulated in Table II.

B. Constraints on Coupling Parameters

Inflaton–SM couplings, whether through decays or scattering, are directly tied to the reheating temperature and are, thus, constrained by the aforementioned combined observations. Figs. 6 and 7 show the 2σ allowed ranges for the Yukawa coupling y_{ϕ} , the bosonic coupling g_{ϕ} , and the scattering coupling σ_{ϕ} in both E- and T-models.

For the *E-model*, y_{ϕ} lies in the range $\sim 10^{-3}$ to a few ⁴, for $w_{\phi} = 0$, while for $w_{\phi} > 1/3$, the allowed range shifts

matter-like reheating case $(w_{\phi} = 0)$, the model predictions lie marginally within the 2σ confidence region for certain values of α . However, the well-known Higgs-Starobinsky model, corresponding to $\alpha = 1$ and n = 1, is excluded at the 2σ level based on the P-ACT-LB-BK18 dataset, as also pointed out in [37]. As w_{ϕ} increases, the predicted values of (n_s, r) shift rightward in the plane, moving into better agreement with observational constraints. This leads to a broader allowed parameter space, not only for inflationary parameters such as α , but also for postinflationary quantities like $T_{\rm RH}$ and the inflaton coupling. However, for stiff equations of state with $w_{\phi} \gtrsim 0.6$, the constraints from PGW overproduction become significant. For example, the upper limit on α for $w_{\phi} = 9/11$ is tightened from 16.5 to 11.7 due to the overproduction of PGWs. The detailed numerical results are presented in Table II for E-model considering different values of w_{ϕ} . Our finding shows that $w_{\phi} = 1/3$ aligns with the 2σ limit of the dataset for $\alpha \in [4, 7]$.

³ In particular, 1σ and 2σ bounds are taken from figure 10 of [24].

⁴ Note that y_{ϕ} can reach values as high as \sim 10 for small w_{ϕ} .

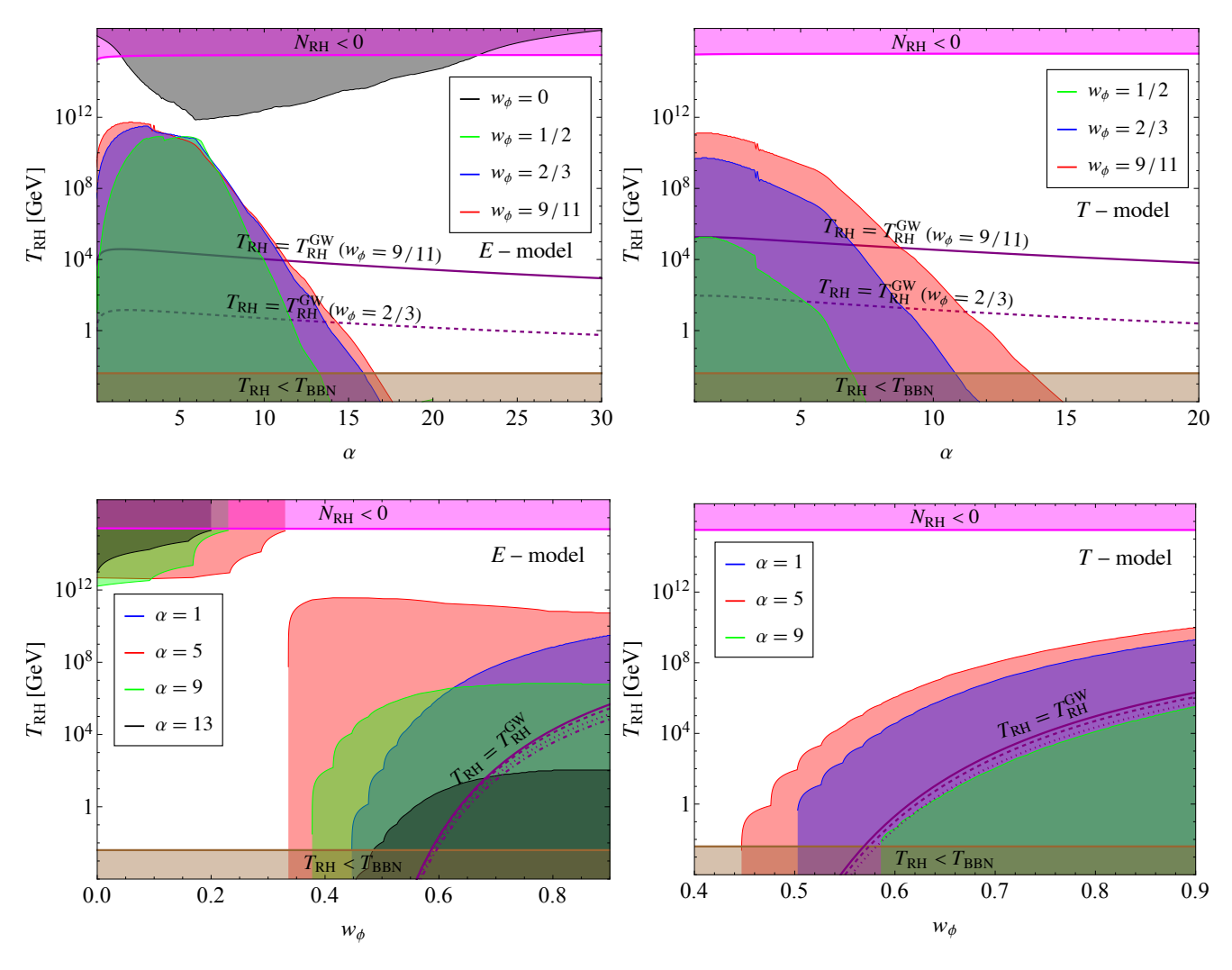


FIG. 5: Constraints on reheating temperature considering 2σ limit of recent P-ACT-LB-BK18 for both E- and T-models. The magenta band shows the region where $N_{\rm RH} < 0$, where the brown band points $T_{\rm RH} < T_{\rm BBN}$. Upper panel: Variation of reheating temperature with α for different w_{ϕ} for both E- (left) and T-model (right). Lower panel: Variation of reheating temperature with w_{ϕ} for different α for both E- (left) and T-model (right).

	range of α		range of $N_{\rm k}$		maximum $T_{\rm RH}$ [GeV]		minimum $T_{\rm RH}$ [GeV]	
$n(w_\phi)$	E-model	T-model	9	T-model	E-model	T-model	E-model	T-model
1(0)	[2.2 - 22.48]	_	[55.886 - 56.635]	_	2.52×10^{15}	_	7.347×10^{11}	_
` '	1.		[58.213 - 61.478]				$T_{ m BBN}$	$T_{ m BBN}$
	-	_	[58.287 - 63.905]					21.30
	1 -		[58.323 - 64.027]	-				5.30×10^4

TABLE II: Limiting values of inflationary model parameters (α, N_k) and bounds on reheating temperature considering 2σ limits of recent P-ACT-LB-BK18 for both E- and T-model.

However, such large couplings may be subject to several theoretical constraints. For instance, the upper bound on the coupling parameter can be set by requiring that inflationary dynamics remain unaffected by inflaton–SM interactions. This bound can

be estimated using the Coleman–Weinberg 1-loop radiative correction formalism, which ensures that quantum corrections remain subdominant [73, 74]. Moreover, very large couplings may also be limited by non-perturbative particle production, which can disrupt the standard perturbative reheating process [8, 54, 75, 76].

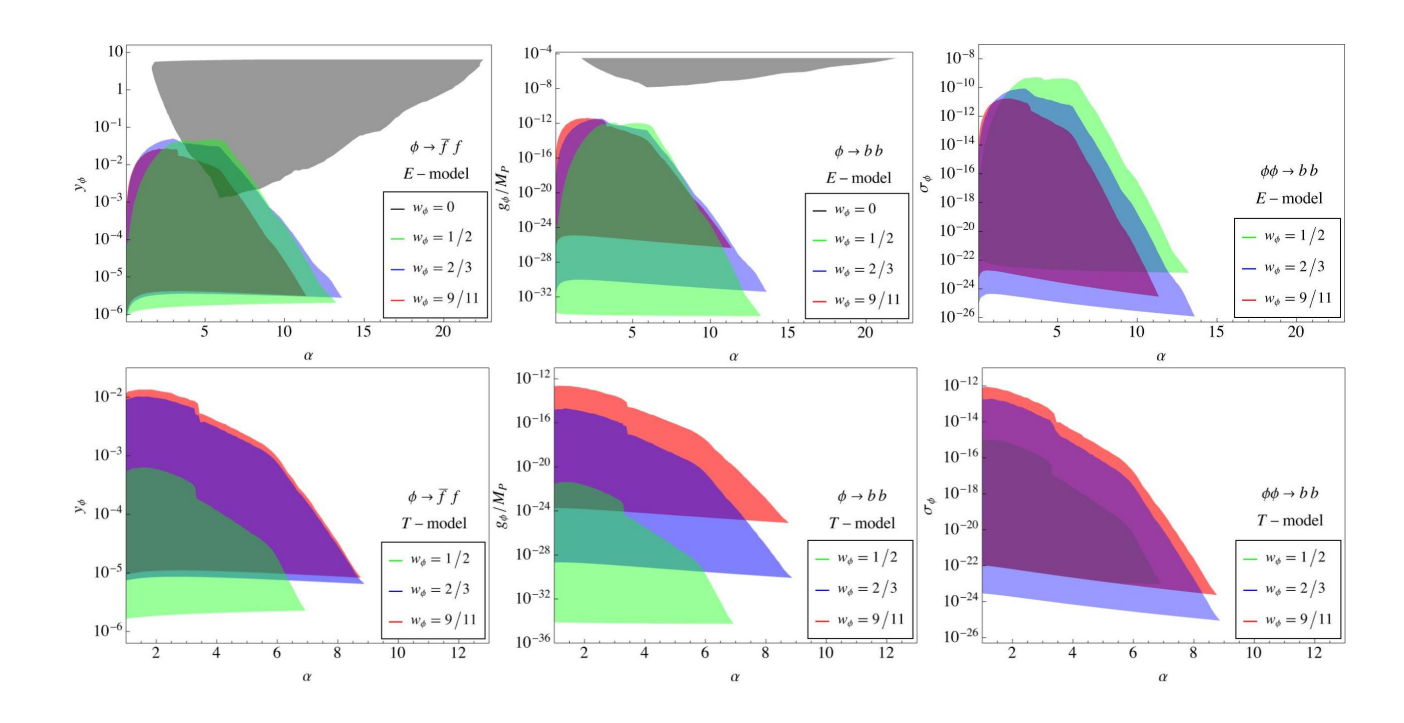


FIG. 6: Constraints on the three different inflaton-SM couplings, considering 2σ limit of recent P-ACT-LB-BK18 for the variation of α with different w_{ϕ} . Upper panel is for E-model, while lower panel representing T-model.

$n(w_{\phi})$	range of y_{ϕ}	range of g_{ϕ}/M_{P}	range of σ_{ϕ}
1(0)	$1.3 \times 10^{-3} - 6.47$	$[2.1 \times 10^{-8} - 3.6 \times 10^{-5}]$	_
3(1/2)	$1.1 \times 10^{-6} - 0.05$	$[10^{-34} - 1.1 \times 10^{-12}]$	$[1.6 \times 10^{-23} - 5.6 \times 10^{-10}]$
5(2/3)	$1.8 \times 10^{-6} - 0.05$	$\left[4.8 \times 10^{-32} - 3.8 \times 10^{-12}\right]$	$[1.4 \times 10^{-26} - 8.3 \times 10^{-11}]$
10(9/11)	$[2 \times 10^{-6} - 0.03]$	$[5 \times 10^{-27} - 3.6 \times 10^{-12}]$	$[3.2 \times 10^{-25} - 1.6 \times 10^{-11}]$

TABLE III: Bounds on inflaton-SM couplings from BBN and $\Delta N_{\rm eff}$ considering the overproduction of PGW under the 2σ limit of recent P-ACT-LB-BK18 for **E-models**.

$n(w_{\phi})$	range of y_{ϕ}	range of $g_{\phi}/M_{\rm P}$	range of σ_{ϕ}
1(0)	_	_	_
3(1/2)	$\left[[1.7 \times 10^{-6} - 6.5 \times 10^{-4}] \right]$	$\left[[6.5 \times 10^{-35} - 5.4 \times 10^{-22}] \right]$	$\left[1 \times 10^{-23} - 9.3 \times 10^{-16}\right]$
5(2/3)	$[6.6 \times 10^{-6} - 10^{-2}]$	$8.7 \times 10^{-31} - 2 \times 10^{-15}$	$[7.6 \times 10^{-26} - 2 \times 10^{-13}]$
10(9/11)	$[8.8 \times 10^{-6} - 1.4 \times 10^{-2}]$	$9.1 \times 10^{-26} - 2.6 \times 10^{-13}$	$[2.5 \times 10^{-24} - 9.8 \times 10^{-13}]$

TABLE IV: Descriptions of the table are same as III, but for T-model.

downward to $\sim [10^{-6}-10^{-2}]$, consistent with the fact that $w_{\phi} > 1/3$ scenarios limit the maximum allowed reheating

temperature. All the three couplings — fermionic (y_{ϕ}) , bosonic (g_{ϕ}) , and scattering (σ_{ϕ}) — become increasingly suppressed for larger values of w_{ϕ} , due to constraints from

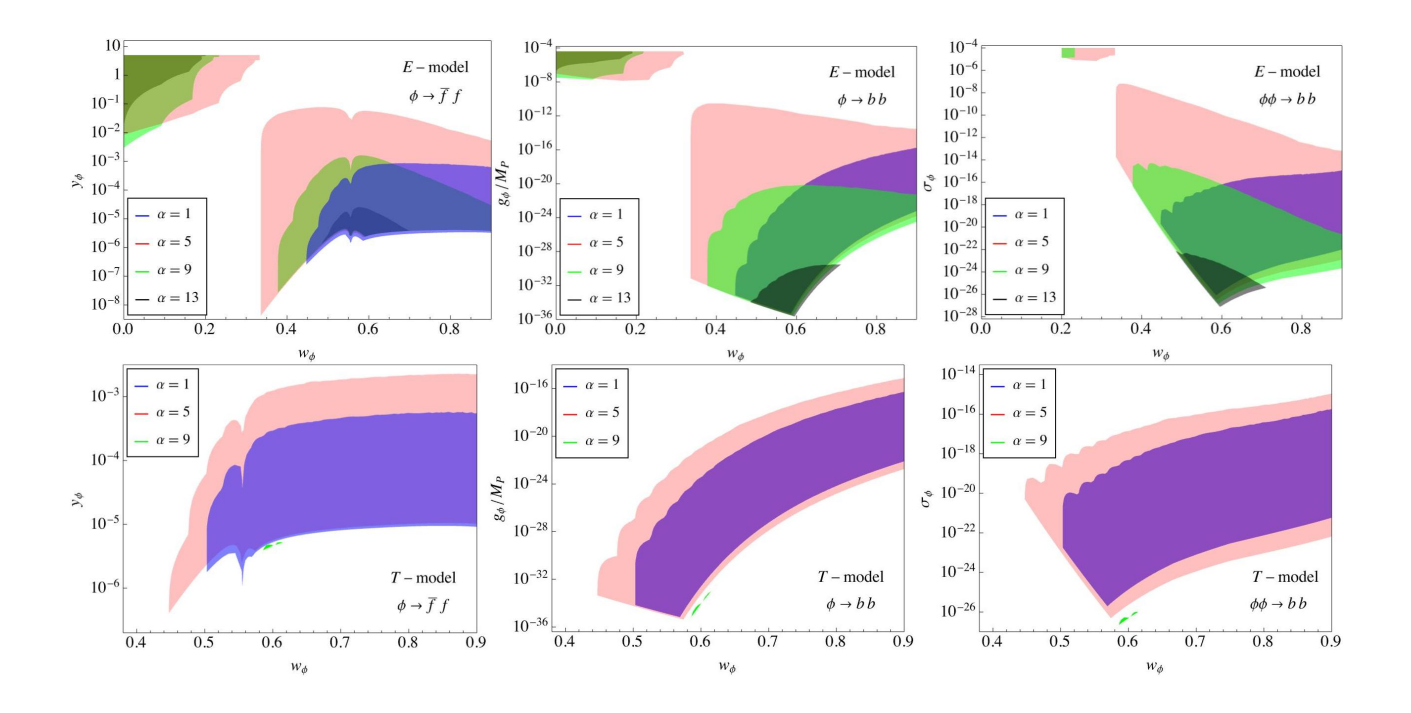


FIG. 7: Description of the figure is same as Fig. 6, but with the variation of w_{ϕ} for different α .

the overproduction of PGWs. Notably, σ_{ϕ} is excluded for $w_{\phi} = 0$, as for $w_{\phi} \lesssim 0.2$, the $\phi \phi \to bb$ process does not lead to successful reheating.

For T-model, all couplings are excluded at 2σ C.L. for $w_{\phi} < 1/3$, with viable ranges appearing only for stiffer EoS ($w_{\phi} \gtrsim 0.44$), where, for instance, y_{ϕ} is constrained to the range $\sim [10^{-6} - 10^{-2}]$, similar to the E-model. Detailed constraints on the coupling parameters for different values of α are tabulated in Tables III and IV, respectively for E- and T-models.

VI. CONCLUSIONS

In this paper, we have studied the impacts of recent P-ACT-LB-BK18, on α -attractor inflationary potentials, focusing specially on both E- and T-models. Our analysis not only places updated constraints on the parameters governing these inflationary potentials but also extends to the post-inflationary reheating phase, where we constrain the reheating temperature and examine three representative inflaton-SM interaction channels: (a) $\phi \to \bar{f} f$, (b) $\phi \to bb$, and (c) $\phi\phi \to bb$. In the following we highlight

our key findings.

- For the E-model, we find that reheating scenarios with an inflaton EoS $w_{\phi} < 1/3$ are allowed within the 2σ C.L. for specific ranges of the α parameter. In particular, matter-like reheating $(w_{\phi} = 0)$ is consistent with the current data for $\alpha \in [2.2, 22.5]$. In contrast, the T-model exhibits a significantly tighter constraint: the entire regime with $w_{\phi} < 1/3$ is excluded at 2σ C.L.
- For E-models, the maximum allowed reheating temperature is around 2.5×10^{15} GeV, determined by $H_{\rm end}$ for instantaneous reheating, particularly for $w_{\phi} < 1/3$. However, as the EoS parameter increases $(w_{\phi} > 1/3)$, the upper bound on the reheating temperature is set by the P-ACT-LB-BK18 dataset. Importantly, we incorporate constraints from the PGW background, which become particularly relevant for stiff EoS $(w_{\phi} > 0.6)$. These constraints effectively raise the lower bound on the reheating temperature beyond the standard BBN requirement. For the E-model, we find that lower value of the reheating temperatures remain above 10^{12} GeV for

 $w_{\phi} < 1/3$. In contrast, for $w_{\phi} > 1/3$, the reheating temperature drops below 5×10^{11} GeV, consistent with the fact that either the BBN or $\Delta N_{\rm eff}$ bound on PGWs sets the lower limit. In comparison, the T-model allows a maximum reheating temperature of only around 10^{11} GeV, since the $w_{\phi} < 1/3$ scenario is not compatible with the aforementioned dataset (see Fig. 5). A comprehensive numerical results are tabulated in Table II.

• Since the inflaton's decay and scattering processes determine the reheating temperature, our analysis provides direct bounds on the associated interaction strengths. For matter-like reheating, we find that inflaton scattering channels are excluded for both Eand T-models as successful reheating is not possible for such coupling when $w_{\phi} = 0$. In the E-model, the allowed range for the Yukawa coupling y_{ϕ} is found to be $y_{\phi} \gtrsim 10^{-3}$ for $w_{\phi} < 1/3$, whereas for $w_{\phi} > 1/3$, the allowed range becomes broader, spanning $10^{-8} \lesssim y_{\phi} \lesssim 10^{-2}$. In the stiff EoS regime, the lower bound is further tightened due to PGW constraints. For g_{ϕ} , we find that $g_{\phi} \gtrsim 10^{-8} M_{\rm P}$ for $w_{\phi} < 1/3$. Notably, for the T-model, no allowed region is found for any of the couplings when $w_{\phi} < 1/3$ (details are illustrated in Figs. 6 and 7). The details of numerical results for the inflaton-SM couplings are tabulated in Tables III (for E-model) and IV (for T-model).

Looking ahead, forthcoming cosmological observations hold great promise for deepening our understanding of the early Universe and physics beyond the Standard Model. In particular, upcoming experiments such as CMB-S4 [77] and LiteBIRD [78] are expected to significantly improve constraints in the (n_s, r) parameter space. These enhanced measurements will offer unprecedented precision in probing the primordial power spectrum and the nature of inflationary dynamics. Such advances will not only refine our knowledge of n_s and r, but also help to distinguish between competing inflationary models. In turn, this will provide valuable insights into the characteristics of the inflaton field and its interactions, potentially revealing new facets of high-energy physics and guiding the construction of viable extensions to the Standard Model. Overall, the synergy between theoretical developments and high-precision observations will continue to play a critical role in shaping our understanding of the early Universe, and we anticipate that the next generation of experiments will mark a transformative step in this ongoing effort.

ACKNOWLEDGEMENTS

The Authors gratefully acknowledge the use of computational facilities at ISI, Kolkata. MRH acknowledges ISI Kolkata for providing financial support through Research Associateship. SP thanks CSIR for financial support through Senior Research Fellowship (File no. 09/093(0195)/2020-EMR-I). DP thanks ISI Kolkata for financial support through Senior Research Fellowship.

- [1] K. N. Abazajian et al. (CMB-S4), (2016), arXiv:1610.02743 [astro-ph.CO].
- [2] Y. Akrami et al. (Planck), Astron. Astrophys. 641, A10 (2020), arXiv:1807.06211 [astro-ph.CO].
- [3] A. H. Guth and S. Y. Pi, Phys. Rev. Lett. 49, 1110 (1982).
- [4] G. Lazarides, in 6th BCSPIN Kathmandu Summer School in Physics: Current Trends in High-Energy Physics and Cosmology (1997) arXiv:hep-ph/9802415.
- [5] A. A. Starobinsky, Phys. Lett. B 117, 175 (1982).
- [6] E. W. Kolb and M. S. Turner, *The Early Universe*, Vol. 69 (Taylor and Francis, 2019).
- [7] Y. Shtanov, J. H. Traschen, and R. H. Brandenberger, Phys. Rev. D 51, 5438 (1995), arXiv:hep-ph/9407247.
- [8] L. Kofman, A. D. Linde, and A. A. Starobinsky, Phys. Rev. D 56, 3258 (1997), arXiv:hep-ph/9704452.
- [9] R. Allahverdi, R. Brandenberger, F.-Y. Cyr-Racine, and A. Mazumdar, Ann. Rev. Nucl. Part. Sci. 60, 27 (2010), arXiv:1001.2600 [hep-th].
- [10] K. D. Lozanov, (2019), arXiv:1907.04402 [astro-ph.CO].
- [11] R. Kallosh, A. Linde, and D. Roest, JHEP 11, 198, arXiv:1311.0472 [hep-th].
- [12] R. Kallosh and A. Linde, JCAP 07, 002, arXiv:1306.5220 [hep-th].
- [13] D. Roest, JCAP **01**, 007, arXiv:1309.1285 [hep-th].

- [14] S. Ferrara, R. Kallosh, A. Linde, and M. Porrati, Phys. Rev. D 88, 085038 (2013), arXiv:1307.7696 [hep-th].
- [15] R. Kallosh, A. Linde, and D. Roest, Phys. Rev. Lett. 112, 011303 (2014), arXiv:1310.3950 [hep-th].
- [16] S. Cecotti and R. Kallosh, JHEP 05, 114, arXiv:1403.2932 [hep-th].
- [17] R. Kallosh, A. Linde, and D. Roest, JHEP 08, 052, arXiv:1405.3646 [hep-th].
- [18] M. Galante, R. Kallosh, A. Linde, and D. Roest, Phys. Rev. Lett. 114, 141302 (2015), arXiv:1412.3797 [hep-th].
- [19] A. A. Starobinsky, Phys. Lett. B 91, 99 (1980).
- [20] A. D. Linde, Phys. Lett. B **129**, 177 (1983).
- [21] J. Ellis, D. V. Nanopoulos, and K. A. Olive, JCAP 10, 009, arXiv:1307.3537 [hep-th].
- [22] R. Kallosh, A. Linde, and D. Roest, JHEP 09, 062, arXiv:1407.4471 [hep-th].
- [23] T. Louis et al. (ACT), (2025), arXiv:2503.14452 [astro-ph.CO].
- [24] E. Calabrese *et al.* (ACT), (2025), arXiv:2503.14454 [astro-ph.CO].
- [25] R. Kallosh, A. Linde, and D. Roest, (2025), arXiv:2503.21030 [hep-th].
- [26] S. Aoki, H. Otsuka, and R. Yanagita, (2025), arXiv:2504.01622 [hep-ph].

- [27] A. Berera, S. Brahma, Z. Qiu, R. O. Ramos, and G. S. Rodrigues, (2025), arXiv:2504.02655 [hep-th].
- [28] C. Dioguardi, A. J. Iovino, and A. Racioppi, (2025), arXiv:2504.02809 [gr-qc].
- [29] I. D. Gialamas, A. Karam, A. Racioppi, and M. Raidal, (2025), arXiv:2504.06002 [astro-ph.CO].
- [30] A. Salvio, (2025), arXiv:2504.10488 [hep-ph].
- [31] I. Antoniadis, J. Ellis, W. Ke, D. V. Nanopoulos, and K. A. Olive, (2025), arXiv:2504.12283 [hep-ph].
- [32] J. Kim, X. Wang, Y.-l. Zhang, and Z. Ren, (2025) arXiv:2504.12035 [astro-ph.CO].
- [33] C. Dioguardi and A. Karam, (2025), arXiv:2504.12937 [gr-qc].
- [34] Q. Gao, Y. Gong, Z. Yi, and F. Zhang, (2025), arXiv:2504.15218 [astro-ph.CO].
- [35] M. He, M. Hong, and K. Mukaida, (2025), arXiv:2504.16069 [astro-ph.CO].
- [36] C. Pallis (2025) arXiv:2504.20273 [hep-ph].
- [37] M. Drees and Y. Xu, (2025), arXiv:2504.20757 [astro-ph.CO].
- [38] M. A. G. Garcia, K. Kaneta, Y. Mambrini, and K. A. Olive, JCAP 04, 012, arXiv:2012.10756 [hep-ph].
- [39] M. A. G. Garcia, K. Kaneta, Y. Mambrini, and K. A. Olive, Phys. Rev. D 101, 123507 (2020), arXiv:2004.08404 [hep-ph].
- [40] M. R. Haque, D. Maity, and R. Mondal, JHEP 09, 012, arXiv:2301.01641 [hep-ph].
- [41] M. Kawasaki, K. Kohri, and N. Sugiyama, Phys. Rev. Lett. 82, 4168 (1999), arXiv:astro-ph/9811437.
- [42] M. Kawasaki, K. Kohri, and N. Sugiyama, Phys. Rev. D 62, 023506 (2000), arXiv:astro-ph/0002127.
- [43] T. Hasegawa, N. Hiroshima, K. Kohri, R. S. L. Hansen, T. Tram, and S. Hannestad, JCAP 12, 012, arXiv:1908.10189 [hep-ph].
- [44] G. F. Giudice, E. W. Kolb, and A. Riotto, Phys. Rev. D 64, 023508 (2001), arXiv:hep-ph/0005123.
- [45] D. Maity and P. Saha, Phys. Rev. D 98, 103525 (2018), arXiv:1801.03059 [hep-ph].
- [46] M. R. Haque and D. Maity, Phys. Rev. D 99, 103534 (2019), arXiv:1902.09491 [hep-th].
- [47] M. R. Haque, D. Maity, and P. Saha, Phys. Rev. D 102, 083534 (2020), arXiv:2009.02794 [hep-th].
- [48] Y. Mambrini and K. A. Olive, Phys. Rev. D 103, 115009 (2021), arXiv:2102.06214 [hep-ph].
- [49] M. R. Haque and D. Maity, Phys. Rev. D 106, 023506 (2022), arXiv:2112.14668 [hep-ph].
- [50] S. Clery, Y. Mambrini, K. A. Olive, and S. Verner, Phys. Rev. D 105, 075005 (2022), arXiv:2112.15214 [hep-ph].
- [51] M. R. Haque and D. Maity, Phys. Rev. D 107, 043531 (2023), arXiv:2201.02348 [hep-ph].
- [52] J. Ellis, M. A. G. Garcia, D. V. Nanopoulos, K. A. Olive, and S. Verner, Phys. Rev. D 105, 043504 (2022), arXiv:2112.04466 [hep-ph].
- [53] M. Drewes, L. Ming, and I. Oldengott, JCAP 05, 081, arXiv:2303.13503 [hep-ph].

- [54] A. Chakraborty, M. R. Haque, D. Maity, and R. Mondal, Phys. Rev. D 108, 023515 (2023), arXiv:2304.13637 [astro-ph.CO].
- [55] L. P. Grishchuk, Zh. Eksp. Teor. Fiz. 67, 825 (1974).
- [56] A. A. Starobinsky, JETP Lett. 30, 682 (1979).
- [57] L. A. Boyle and P. J. Steinhardt, Phys. Rev. D 77, 063504 (2008), arXiv:astro-ph/0512014.
- [58] Y. Watanabe and E. Komatsu, Phys. Rev. D 73, 123515 (2006), arXiv:astro-ph/0604176.
- [59] K. Saikawa and S. Shirai, JCAP 05, 035, arXiv:1803.01038 [hep-ph].
- [60] C. Caprini and D. G. Figueroa, Class. Quant. Grav. 35, 163001 (2018), arXiv:1801.04268 [astro-ph.CO].
- [61] N. Bernal and F. Hajkarim, Phys. Rev. D 100, 063502 (2019), arXiv:1905.10410 [astro-ph.CO].
- [62] M. R. Haque, D. Maity, T. Paul, and L. Sriramkumar, Phys. Rev. D 104, 063513 (2021), arXiv:2105.09242 [astroph.CO].
- [63] S. Maity, N. Bhaumik, M. R. Haque, D. Maity, and L. Sriramkumar, JCAP 01, 118, arXiv:2403.16963 [astro-ph.CO].
- [64] S. Maity and M. R. Haque, (2024), arXiv:2407.18246 [astro-ph.CO].
- [65] A. Ghoshal, D. Paul, and S. Pal, JHEP 12, 150, arXiv:2405.06741 [hep-ph].
- [66] B. Barman, A. Ghoshal, B. Grzadkowski, and A. Socha, JHEP 07, 231, arXiv:2305.00027 [hep-ph].
- [67] B. Barman, S. Jyoti Das, M. R. Haque, and Y. Mambrini, Phys. Rev. D 110, 043528 (2024), arXiv:2403.05626 [hep-ph].
- [68] M. Drewes, J. U. Kang, and U. R. Mun, JHEP 11, 072, arXiv:1708.01197 [astro-ph.CO].
- [69] G. German, JCAP 09, 017, arXiv:2105.05426 [astro-ph.CO].
- [70] L. H. Ford, Phys. Rev. D **35**, 2955 (1987).
- [71] L. Dai, M. Kamionkowski, and J. Wang, Phys. Rev. Lett. 113, 041302 (2014), arXiv:1404.6704 [astro-ph.CO].
- [72] J. L. Cook, E. Dimastrogiovanni, D. A. Easson, and L. M. Krauss, JCAP 04, 047, arXiv:1502.04673 [astro-ph.CO].
- [73] S. R. Coleman and E. J. Weinberg, Phys. Rev. D 7, 1888 (1973).
- [74] M. Drees and Y. Xu, JCAP 09, 012, arXiv:2104.03977 [hep-ph].
- [75] P. B. Greene, L. Kofman, A. D. Linde, and A. A. Starobinsky, Phys. Rev. D 56, 6175 (1997), arXiv:hep-ph/9705347.
- [76] P. B. Greene and L. Kofman, Phys. Rev. D 62, 123516 (2000), arXiv:hep-ph/0003018.
- [77] K. Abazajian et al. (CMB-S4), Astrophys. J. 926, 54 (2022), arXiv:2008.12619 [astro-ph.CO].
- [78] E. Allys et al. (LiteBIRD), PTEP 2023, 042F01 (2023), arXiv:2202.02773 [astro-ph.IM].